Series Solutions of Magnetohydrodynamic Peristaltic Flow of a Jeffrey Fluid in Eccentric Cylinders

R. Ellahi[1,2,*], *A. Riaz*[2], *S. Nadeem*[3], *M. Mushtaq*[4]

[1]Department of Mechanical Engineering, University of California Riverside, USA
[2]Faculty of Basic and Applied Sciences, IIU Islamabad, Pakistan
[3]Faculty of Natural Sciences, Quaid-i-Azam University Islamabad, Pakistan
[4]Department of Mathematics, University of Engineering & Technology, Lahore, Pakistan

Abstract: In this article, the mathematical modelling on magnetohydrodynamic peristaltic flow of Jeffrey fluid in the gap between two eccentric tubes has been discussed in the presence of applied magnetic field. Geometrically, we considered two eccentric tubes in which the inner tube is rigid while the tube at the outer side has a sinusoidal wave propagating along the wall. The governing equations for Jeffrey fluid in a cylindrical coordinates for three dimensional flow are given. The approximations of low Reynolds number and long wavelength have been employed to reduce the highly nonlinear partial differential equations. The problem has been solved with the help of homotopy perturbation method alongwith eigen function expansion method. The graphs of pressure rise, pressure gradient and velocity (for two and three dimensional flow) have been drawn. The streamlines have also been presented to discuss the trapping bolus discipline.

Keywords: Peristaltic flow, Eccentric cylinders, Jeffrey fluid, Magnetohydrodynamic (MHD),Nonlinear partial differential equations, Analytical solutions, HPM.

1 Introduction

Peristaltic pumping is a phenomenon in which fluid transport happens when a gradually wave of area contraction or expansion propagates along the length of distensible duct. It is an instinctive property of many biological disciplines possessing smooth muscle tubes which helps in flowing biofluids by its propulsive movements and is found in the transport of urine from kidney to the bladder, the movement of chyme in the gastro-intestinal tract, intra-uterine fluid motion, vasomotion of the small blood vessels and in many other glandular ducts. The mechanism of peristaltic transport has been exploited for industrial applications like sanitary fluid transport, blood pumps in heart lung machine and transport of corrosive fluids where the contact of the fluid with the machinery parts is prohibited. Peristaltic transport of a Newtonian fluid in a vertical asymmetric channel with heat transfer and porous medium have been analyzed by Srinivas and Gayathri [1] . Kothandapani and Srinivas [2] have examined the peristaltic transport of a

Jeffrey fluid under the effect of magnetic field in asymmetric channel under the assumptions of long wavelength and low Reynolds number. A number of analytical and numerical studies [3,4,5,6] of peristaltic flows of different fluids have been reported. Mekheimer [7] measured the effect of magnetic field on peristaltic transport of blood in a non-uniform two dimensional channel, when blood is characterized by a couple stress fluid. In recent years, peristaltic transport through a concentric annulus has obtained much concentration. A lot of investigations are available in the literature to study the effect of an endoscope on peristaltic motion of Newtonian and non-Newtonian fluids [8,9,10,11,12] The eccentric annulus is normally not easy to discuss even without peristalsis. There are only a few studies take into attention the effect of the eccentricity attribute [13,14].

To be more specific, only one study is available which discusses the peristaltic flow of a viscous fluid through eccentric cylinders [15] To the best of author's knowledge, the peristaltic flow of non-Newtonian fluid through the eccentric cylinders has not been explored so

* Corresponding author e-mail: rellahi@engr.ucr.edu, rahmatellahi@yahoo.com

for. Therefore, the main purpose of the present paper is to discuss the effect of peristaltic transport on the Jeffrey fluid flow in the gap between two eccentric tubes, the outer tube gets the sinusoidal wave propagating down the wall and the inner tube is rigid. A motivation of the present work is the anticipation that such a problem will be beneficial in many clinical applications. This analysis gives a better judgement for the speed of injection and the fluid flow characteristics within the syringe. Also, the injection can be carried out more proficiently and pain of the patient can be extenuated.

2 Mathematical formulation of the problem

The MHD flow of an incompressible non-Newtonian Jeffrey fluid is considered here. The flow geometry is described as the inner tube is rigid and sinusoidal wave is travelling at the outer tube down its wall. The radius of the inner tube is δ but we require to consider the fluid motion to the centre of the outer tube. The centre of the inner tube is now at the position $r = \varepsilon$, $z = 0$, where r and z are coordinates in the cross-section of the pipe as shown in the Fig. 1. The radially varying magnetic field is applied normally to the direction of the flow. Then the boundary of the inner tube is described to order ε by $r_1 = \delta + \varepsilon \cos \theta$, where ε is the parameter that controls the eccentricity of the inner tube position. The geometry of the walls is visualized in Fig. 1.

The equations for the radii are

$$r_1 = \delta + \varepsilon \cos \theta,$$

$$r_2 = a + b \cos \left[\frac{2\pi}{\lambda} (z - ct) \right],$$

where δ and a are the radii of the inner and outer tubes, b is amplitude of the wave, λ is the wavelength, c is the propagation velocity and t is the time. the problem has been considered in the system of cylindrical coordinates (r, θ, z) as radial, azimuthal and axial coordinates, respectively.

The continuity and momentum equations for an incompressible Jeffrey fluid are described as follow

$$\text{div} \, \mathbf{V} = 0, \tag{1}$$

$$\rho \frac{d\mathbf{V}}{dt} = -\nabla p + \text{div} \, \mathbf{S} + \mathbf{J} \times \mathbf{B}, \tag{2}$$

where ρ is the density, d/dt is the material time derivative, $\mathbf{V}$ is the velocity field, p is the pressure, $\mathbf{S}$ is the stress tensor for Jeffrey fluid, $\mathbf{J}$ is the electric current density, $\mathbf{B}$ is the total magnetic field, $\mathbf{b}$ is the body force. Note that considering the cylindrical coordinates system for the velocity field $\mathbf{V} = (v, w, u)$ and in the absence of body force, equations (1) and (2) correspondingly take the following form

$$\frac{\partial u}{\partial z} + \frac{\partial v}{\partial r} + \frac{v}{r} + \frac{1}{r} \frac{\partial w}{\partial \theta} = 0, \tag{3}$$
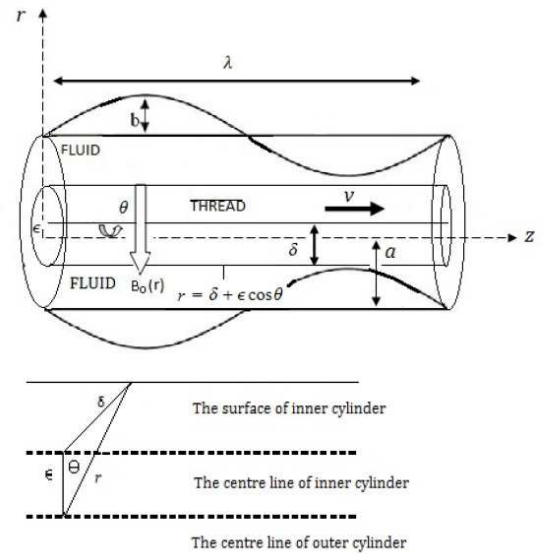

Fig. 1: The simplified model of geometry of the problem.

$$\rho \left[\frac{\partial v}{\partial t} + u \frac{\partial v}{\partial z} + v \frac{\partial v}{\partial r} + \frac{w}{r} \frac{\partial v}{\partial \theta} - \frac{w^2}{r} \right] = -\frac{\partial p}{\partial r} + \frac{1}{r} \frac{\partial}{\partial r} (r S_{rr}) + \frac{1}{r} \frac{\partial}{\partial \theta} (S_{r\theta}) + \frac{\partial}{\partial z} (S_{rz}) - \frac{S_{\theta\theta}}{r}, \tag{4}$$

$$\rho \left[\frac{\partial w}{\partial t} + u \frac{\partial w}{\partial z} + v \frac{\partial w}{\partial r} + \frac{w}{r} \frac{\partial w}{\partial \theta} - \frac{wv}{r} \right] = -\frac{1}{r} \frac{\partial p}{\partial \theta} + \frac{1}{r^2} \frac{\partial}{\partial r} (r^2 S_{r\theta}) + \frac{1}{r} \frac{\partial}{\partial \theta} (S_{\theta\theta}) + \frac{\partial}{\partial z} (S_{\theta z}), \tag{5}$$

$$\rho \left[\frac{\partial u}{\partial t} + u \frac{\partial u}{\partial z} + v \frac{\partial u}{\partial r} + \frac{w}{r} \frac{\partial u}{\partial \theta} \right] = -\frac{\partial p}{\partial z} + \frac{1}{r} \frac{\partial}{\partial r} (r S_{rz}) + \frac{1}{r} \frac{\partial}{\partial \theta} (S_{\theta z}) + \frac{\partial}{\partial z} (S_{zz}) - \sigma B_0^2(r) u, \tag{6}$$

where v, w and u are the velocity components in r, θ and $z-$directions, respectively, μ is the viscosity, S_{rr}, $S_{r\theta}$, S_{rz}, $S_{\theta\theta}$, $S_{\theta z}$ and S_{zz} are stresses for Jeffrey fluid which can be computed with the help of following stress [11]

$$\mathbf{S} = \frac{\mu}{1 + \lambda_1} \left(\dot{\gamma} + \lambda_2 \ddot{\gamma} \right).$$

According to the flow geometry, the boundary conditions are defined as

$$u = 0, \quad \text{at } r = r_2, \tag{7}$$

$$u = V, \quad \text{at } r = r_1, \tag{8}$$

where V is the velocity of the inner tube. The velocity component in the azimuthal direction is assumed to be unaffected, so the velocity field is taken as $(v, 0, u)$. The governing equations are made dimensionless by using the following non-dimensional parameters

$$p' = \frac{a^2}{\mu c \lambda} p, \; u' = \frac{u}{c}, \; v' = \frac{\lambda}{ac} v, \; t' = \frac{c}{\lambda} t, \; r_1' = \frac{r_1}{a}, \; \phi = \frac{b}{a}, \; \delta' = \frac{\delta}{a}, \; \varepsilon' = \frac{\varepsilon}{a}, \; \delta_0 = \frac{a}{\lambda}, \; z' = \frac{z}{\lambda},$$

$$r_2' = \frac{r_2}{a}, \; \text{Re} = \frac{\rho c a}{\mu}, \; \overline{M}^2(r) = \frac{\sigma B_0^2(r) a^2}{\mu}, \; \theta' = \theta, \; V' = \frac{V}{c},$$

where ϕ is the amplitude ratio, M is the MHD parameter, Re is the Reynold's number, δ_0 is the dimensionless wave number, ε is the eccentricity parameter. After using the above dimensionless parameters, the governing equations (after dropping dashes) are reduced to the following form

$$\frac{\partial v}{\partial r} + \frac{v}{r} + \frac{\partial u}{\partial z} = 0, \tag{9}$$

$$\text{Re}\,\delta_0^3 \left[\frac{\partial v}{\partial t} + u\frac{\partial v}{\partial z} + v\frac{\partial v}{\partial r} \right] = -\frac{\partial p}{\partial r} + \frac{\delta}{r}\frac{\partial}{\partial r}(rS_{rr}) + \frac{\delta}{r}\frac{\partial}{\partial \theta}(S_{r\theta}) + \delta^2 \frac{\partial}{\partial z}(S_{rz}) - \delta \frac{S_{\theta\theta}}{r}, \tag{10}$$

$$0 = -\frac{1}{r}\frac{\partial p}{\partial \theta} + \frac{\delta}{r^2}\frac{\partial}{\partial r}\left(r^2 S_{r\theta}\right) + \frac{\delta}{r}\frac{\partial}{\partial \theta}(S_{\theta\theta}) + \delta^2 \frac{\partial}{\partial z}(S_{\theta z}), \tag{11}$$

$$\text{Re}\,\delta_0 \left[\frac{\partial u}{\partial t} + u\frac{\partial u}{\partial z} \right] = -\frac{\partial p}{\partial z} + \frac{1}{r}\frac{\partial}{\partial r}(rS_{rz}) + \frac{1}{r}\frac{\partial}{\partial \theta}(S_{\theta z}) + \delta\frac{\partial}{\partial z}(S_{zz}) - \overline{M}^2(r)u. \tag{12}$$

The components of non-dimensional stresses for Jeffrey fluid are evaluated as

$$S_{rr} = \frac{2\delta}{1+\lambda_1}\left(1 + \frac{\lambda_2 c\delta}{a}\left(\frac{\partial}{\partial t} + v\frac{\partial}{\partial r} + u\frac{\partial}{\partial z}\right)\right)\frac{\partial v}{\partial r},$$

$$S_{r\theta} = \frac{\delta}{1+\lambda_1}\left(1 + \frac{\lambda_2 c\delta}{a}\left(\frac{\partial}{\partial t} + v\frac{\partial}{\partial r} + u\frac{\partial}{\partial z}\right)\right)\frac{1}{r}\frac{\partial v}{\partial \theta},$$

$$S_{rz} = \frac{1}{1+\lambda_1}\left(1 + \frac{\lambda_2 c\delta}{a}\left(\frac{\partial}{\partial t} + v\frac{\partial}{\partial r} + u\frac{\partial}{\partial z}\right)\right)\left(\delta^2 \frac{\partial v}{\partial z} + \frac{\partial u}{\partial r}\right),$$

$$S_{\theta\theta} = \frac{2\delta}{1+\lambda_1}\left(1 + \frac{\lambda_2 c\delta}{a}\left(\frac{\partial}{\partial t} + v\frac{\partial}{\partial r} + u\frac{\partial}{\partial z}\right)\right)\frac{v}{r},$$

$$S_{\theta z} = \frac{1}{1+\lambda_1}\left(1 + \frac{\lambda_2 c\delta}{a}\left(\frac{\partial}{\partial t} + v\frac{\partial}{\partial r} + u\frac{\partial}{\partial z}\right)\right)\frac{1}{r}\frac{\partial u}{\partial \theta},$$

$$S_{zz} = \frac{2\delta}{1+\lambda_1}\left(1 + \frac{\lambda_2 c\delta}{a}\left(\frac{\partial}{\partial t} + v\frac{\partial}{\partial r} + u\frac{\partial}{\partial z}\right)\right)\frac{\partial u}{\partial z}. \tag{13}$$

Using the long wavelength approximation ($\delta_0 \to 0$) and taking $\overline{M}(r) = \frac{M}{r}$, the governing equations $(10-12)$ are simplified to the following form

$$\frac{\partial p}{\partial r} = 0, \tag{14}$$

$$\frac{\partial p}{\partial \theta} = 0, \tag{15}$$

$$(1+\lambda_1)\frac{\partial p}{\partial z} = \frac{\partial^2 u}{\partial r^2} + \frac{1}{r}\frac{\partial u}{\partial r} + \frac{1}{r^2}\frac{\partial^2 u}{\partial \theta^2} - (1+\lambda_1)\frac{M^2}{r^2}u$$

or

$$(1+\lambda_1)\frac{\partial p}{\partial z} = \frac{\partial^2 u}{\partial r^2} + \frac{1}{r}\frac{\partial u}{\partial r} + \frac{1}{r^2}\frac{\partial^2 u}{\partial \theta^2} - \frac{N^2}{r^2}u, \tag{16}$$

where $N = M\sqrt{1+\lambda_1}$. Eqs. (14) and (15) show that p is not a function of r and θ. The corresponding boundary conditions in non-dimensional form are

$$u = 0, \quad \text{at } r = r_2 = 1 + \phi\cos[2\pi(z-t)], \tag{17}$$

$$u = V, \quad \text{at } r = r_1 = \delta + \varepsilon\cos\theta. \tag{18}$$

3 Solution of the problem

Solution of the above boundary value problem is evaluated by using homotopy perturbation method $[16-17]$. The homotopy equation for the given problem is defined as

$$H(u,q) = (1-q)(\mathscr{L}[\tilde{u}] - \mathscr{L}[\tilde{u}_0]) + q\left(\mathscr{L}[\tilde{u}] + \frac{1}{r^2}\frac{\partial^2 \tilde{u}}{\partial \theta^2} - (1+\lambda_1)\frac{dp}{dz}\right) = 0, \tag{19}$$

where $\mathscr{L}$, the linear operator is assumed to be $\mathscr{L} = \frac{\partial^2}{\partial r^2} + \frac{1}{r}\frac{\partial}{\partial r} - \frac{N^2}{r^2}$. We define the following initial guess

$$\tilde{u}_0 = V\sinh\left(N\left(\log[r] - \log[r_2]\right)\right)\operatorname{csch}\left(N\left(\log[r_1] - \log[r_2]\right)\right). \tag{20}$$

Now we describe

$$\tilde{u}(r,\theta,z,t,q) = u_0 + qu_1 + \ldots \tag{21}$$

Using the above equation into Eq. (19) and then taking the terms of first two orders, we get the following problems alongwith corresponding boundary conditions

Zeroth order system

$$\mathscr{L}[u_0] - \mathscr{L}[\tilde{u}_0] = 0, \tag{22}$$

$$u_0 = 0, \quad \text{at } r = r_2, \tag{23}$$

$$u_0 = V, \quad \text{at } r = r_1. \tag{24}$$

The solution of the above zeroth order system can be obtained by using Eq. (20) and is directly written as

$$u_0(r,\theta,z,t,q) = \tilde{u}_0 = V\sinh\left(N\left(\log[r] - \log[r_2]\right)\right)\operatorname{csch}\left(N\left(\log[r_1] - \log[r_2]\right)\right). \tag{25}$$

First order system

$$\mathscr{L}[u_1] + \mathscr{L}[\tilde{u}_0] + \frac{1}{r^2}\frac{\partial^2 u_0}{\partial \theta^2} - (1+\lambda_1)\frac{dp}{dz} = 0 \tag{26}$$

or

$$\frac{\partial^2 u_1}{\partial r^2} + \frac{1}{r}\frac{\partial u_1}{\partial r} - \frac{N^2}{r^2}u_1 = (1+\lambda_1)\frac{dp}{dz} - \frac{1}{r^2}\frac{\partial^2 u_0}{\partial \theta^2}, \tag{27}$$

$$u_1 = 0, \quad \text{at } r = r_2, \tag{28}$$

$$u_1 = 0, \quad \text{at } r = r_1. \tag{29}$$

The solution of the above linear ordinary differential equation is found as

$$u_1 = \frac{1}{4N(N^2-4)}\left(\operatorname{csch}\left(N\log\left[\frac{r_1}{r_2}\right]\right)\left(\left(-4N\frac{dp}{dz}r_2^2 + f\left(N^2-4\right)\log\left[\frac{r_1}{r_2}\right]\right) \times \right.\right.$$
$$\sinh\left(N\log\left[\frac{r}{r_1}\right]\right) - f\left(N^2-4\right)\log\left[\frac{r}{r_1}\right]\sinh\left(N\log\left[\frac{r_1}{r_2}\right]\right) + 4N\frac{dp}{dz}\left(r_1^2\sinh\left(N\log\left[\frac{r}{r_2}\right]\right) - \right.$$
$$r^2\sinh\left(N\log\left[\frac{r_1}{r_2}\right]\right) - 4N\frac{dp}{dz}\left(r_2^2\sinh\left(N\log\frac{r}{r_1}\right) - r_1^2\sinh\left(N\log\frac{r}{r_2}\right) + \right.$$
$$\left.\left.\left.r^2\sinh\left(N\log\frac{r_1}{r_2}\right)\right)\lambda_1\right)\right), \tag{30}$$

where

$$f = \frac{1}{(\delta + \varepsilon\cos\theta)^2}\left(NV\varepsilon\,\mathrm{csch}\left(N\log\left[\frac{\delta + \varepsilon\cos\theta}{r_2}\right]\right)\left((\varepsilon + \delta\cos\theta)\coth\left(N\left(\log\left[\frac{\delta + \varepsilon\cos\theta}{r_2}\right]\right)\right)\right) + \right.$$
$$\left. N\varepsilon\left(1 + 2\,\mathrm{csch}^2\left(N\left(\log\left[\frac{\delta + \varepsilon\cos\theta}{r_2}\right]\right)\right)\right)\sin^2\theta\right)\right).$$

Now for $q \to 1$, we approach the final solution. So from Eq. (21), we get

$$u(r,\theta,z,t) = u_0 + u_1, \tag{31}$$

where u_0 and u_1 are defined in Eqs. (25) and (30). The instantaneous volume flow rate $Q(z,t)$ is given by

$$\overline{Q}(z,t) = 2\pi\int_{r_1}^{r_2} rudr, \tag{32}$$

$$\overline{Q}/2\pi = \frac{1}{4N(N^2-4)^2}\left(\left(N^2+4\right)\left(2fr_2^2 + N\frac{dp}{dz}\left(r_1^4-r_2^4\right)\right) + 8N\left(N^2-4\right)r_1^2V - 2f\left(N^2+4\right)r_1^2\times\right.$$
$$\cosh\left(N\log\left[\frac{r_1}{r_2}\right]\right) + 2N\,\mathrm{csch}\left(N\log\left[\frac{r_1}{r_2}\right]\right)\left(2Nr_2^2\left(2\frac{dp}{dz}r_1^2 + (N^2-4)V\right) - f\left(N^2-4\right)r_1^2\times\right.$$
$$\left.\log\left[\frac{r_1}{r_2}\right]\right) - 2N\coth\left(N\log\left[\frac{r_1}{r_2}\right]\right)\left(2N\left(\frac{dp}{dz}\left(r_1^4+r_2^4\right) + (N^2-4)r_1^2V\right) - f\left(N^2-4\right)r_2^2\times\right.$$
$$\log\left[\frac{r_1}{r_2}\right]\right) + 8fNr_1^2\sinh\left(N\log\frac{r_1}{r_2}\right) + N\frac{dp}{dz}\left((N^2+4)\left(r_1^4-r_2^4\right) - 4N\left(r_1^4+r_2^4\right)\coth\left(N\log\frac{r_1}{r_2}\right) + \right.$$
$$\left.8Nr_1^2r_2^2\,\mathrm{csch}\left(N\log\frac{r_1}{r_2}\right)\right)\lambda_1\right). \tag{33}$$

The mean volume flow rate $\overline{Q}$ over one period is given as Mekheimer et. al. [15]

$$\overline{Q}(z,t) = \frac{Q}{\pi} - \frac{\phi^2}{2} + 2\phi\cos[2\pi(z-t)] + \phi^2\cos^2[2\pi(z-t)], \tag{34}$$

where Q is the time average of the flow over one period of the wave. Now we can evaluate pressure gradient dp/dz by solving Eqs. (33) and (34) and is obtained as

$$\frac{dp}{dz} = \left(2\left(-4f\pi r_2^2 + N\left(2\left(N^2-4\right)^2\overline{Q} + \pi\left(fNr_2^2 - 4\left(N^2-4\right)r_1^2V\right)\right) + N\left(N^2-4\right)^2\pi\phi\times\right.\right.$$
$$\left(4\cos[2\pi(z-t)] + \phi\cos[4\pi(z-t)]\right) + f\left(N^2+4\right)\pi r_1^2\cosh\left(N\log\left[\frac{r_1}{r_2}\right]\right) + $$
$$N\pi\,\mathrm{csch}\left(N\log\frac{r_1}{r_2}\right)\left(2fr_2^2 - 2N\left(N^2-4\right)r_2^2V + fr_1^2\left(2\cosh\left(2N\log\frac{r_2}{r_1}\right) + \right.\right.$$
$$\left.\left.\left.\left(N^2-4\right)\log\frac{r_1}{r_2}\right) + \left(N^2-4\right)\cosh\left(N\log\left[\frac{r_1}{r_2}\right]\right)\left(2Nr_1^2V + fr_2^2\log\left[\frac{r_2}{r_1}\right]\right)\right)\right)\right)/$$
$$\left(N\pi\left(\left(N^2+4\right)\left(r_1^4-r_2^4\right) - 4N\left(r_1^4+r_2^4\right)\coth\left(N\log\left[\frac{r_1}{r_2}\right]\right) + \right.\right.$$
$$\left.\left.8Nr_1^2r_2^2\,\mathrm{csch}\left(N\log\left[\frac{r_1}{r_2}\right]\right)\right)(1+\lambda_1)\right). \tag{35}$$

The pressure rise $\Delta p(t)$ in non-dimensional form is defined as

$$\Delta p(t) = \int_0^1 \frac{\partial p}{\partial z}dz. \tag{36}$$

4 Results and discussions

The analytical and numerical results obtained above for the given analysis are discussed graphically in this section. The comparison table and graph of the results found in the present case with that of the previous one are presented. The graphical treatment for the data of pressure rise Δp, pressure gradient dp/dz and velocity

profile $u(r,\theta,z,t)$ with the variation of all emerging dimensionless parameters like time t, flow rate Q, amplitude ratio ϕ, the velocity of the inner tube V, the eccentricity parameter ε, Jeffrey fluid parameter λ_1 and the MHD parameter M has been analyzed. In the end, the stream lines observing the peristaltic flow are drawn for the parameters M, Q, λ_1 and ϕ while other parameters remain fixed.

Table. 1 is shown to see the matching of results for the current case and the previously discussed case.

Table 1: Variation of velocity distribution for r.

|	Mekheimer et al. [15]	Present work	
r	$u(r,\theta,z,t)$	$u(r,\theta,z,t)\,for\,M=0,\lambda_1=0$	$u(r,\theta,z,t)\,for\,M=0.5,\lambda_1=1.0$
0.20	0.1000	0.1000	0.1000
0.25	0.1093	0.1081	0.0969
0.30	0.1119	0.1116	0.0944
0.35	0.1119	0.1120	0.0918
0.40	0.1096	0.1099	0.0887
0.45	0.1054	0.1057	0.0848
0.50	0.0995	0.0997	0.0801
0.55	0.0919	0.0920	0.0743
0.60	0.0829	0.0829	0.0674
0.65	0.0724	0.0723	0.0593
0.70	0.0606	0.0604	0.0501
0.75	0.0474	0.0472	0.0395
0.80	0.0329	0.0327	0.0277
0.85	0.0171	0.0170	0.0145
0.90	0.0000	0.0000	0.0000

The comparison graph for the values obtained in present work with the results of Mekheimer et. al. [15] is displayed in Fig. 2. The graphs for the pressure rise $\Delta p(t)$ versus flow rate Q under the effects of given parameters are drawn in Figs. 3-7. These graphs show the pumping regions, that is, the peristaltic pumping $(Q > 0, \Delta p > 0)$, the augmented pumping $(Q > 0, \Delta p < 0)$ and the retrograde pumping $(Q < 0, \Delta p > 0)$. The pressure gradient dp/dz against the the coordinate z with the variation of pertinent parameters are shown in Figs. 8-12. The velocity field $u(r,\theta,z,t)$ versus the radial coordinate r is plotted in Figs. 13-17 for both two and three dimensions. The stream line graphs are shown in Figs. 18-21.
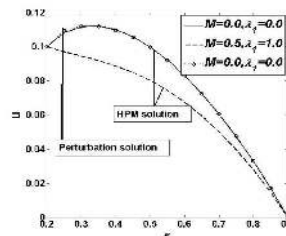
Fig. 2: Variation of velocity distribution with r for fixed $\delta = 0.1$, $\theta = 0.01$, $\phi = 0.1$, $z = 0$, $t = 0.5$, $V = 0.1$, $\varepsilon = 0.1$, $Q = 0.6$.

It is observed from Fig. 2 that the results obtained in the present case are in good agreement with that of

previous calculations in most part of the geometry. It is also observed that the presence of magnetic field for Jeffrey fluid causes to slow down the flow.
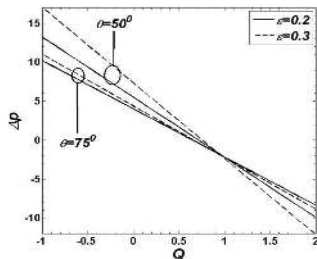
Fig. 3: Variation of pressure rise Δp with Q for fixed $\delta = 0.1$, $\phi = 0.2$, $t = 0.1$, $M = 0.5$, $V = 0.5$, $\lambda_1 = 1.5$.

Fig. 3 is plotted to see the variation of pressure rise for different values of the eccentricity parameter ε and the angle θ while all other parameters are kept fixed. It is observed that peristaltic pumping region is in between $Q \in [0, 0.9]$, augmented pumping is in $Q \in [0.9, 2]$ and retrograde pumping part is $Q \in [-1, 0]$. It is also observed from this graph that the pressure rise increases with the variation of ε but decreases with the angle θ in between the region $Q \in [-1, 0.9]$ and opposite behavior is seen in the remaining part. The graph of pressure rise for the parameter M and δ is plotted in Fig. 4.
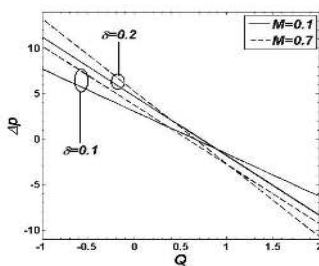
Fig. 4: Variation of pressure rise Δp with Q for fixed $\varepsilon = 0.01$, $\phi = 0.2$, $t = 0.1$, $\theta = 50^0$, $V = 0.5$, $\lambda_1 = 1.5$.

The peristaltic pumping occurs in the region $Q \in [0, 0.6]$, augmented pumping is in $Q \in [0.6, 2]$ and retrograde pumping part is $Q \in [-1, 0]$. It is clear that the similar behavior is seen in this case for the parameter M but the opposite attitude is observed with the variation of δ as compared to that of ε and θ. It tells that the flow rate decreases with M while increases with δ, so this shows that the back flow increases and decreases with M and δ, respectively.

Fig. 5 shows that the peristaltic pumping part is $Q \in [0, 0.3]$, while augmented and retrograde pumping regions are $Q \in [0.3, 2]$ and $Q \in [-1, 0]$, respectively. The variation
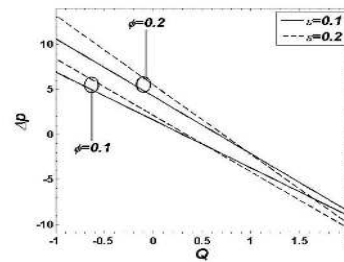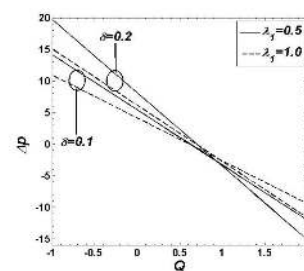

Fig. 5: Variation of pressure rise Δp with Q for fixed $\delta = 0.1$, $M = 0.5$, $t = 0.1$, $\theta = 50^0$, $V = 0.5$, $\lambda_1 = 1.5$.

of pressure rise ∇p for V is similar to that of M (See Fig. 6).
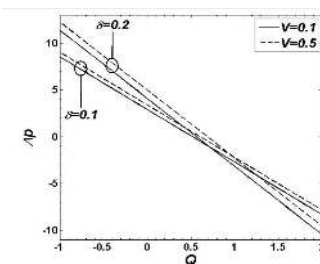
Fig. 6: Variation of pressure rise Δp with Q for fixed $\varepsilon = 0.01$, $M = 0.5$, $t = 0.1$, $\theta = 50^0$, $\phi = 0.2$, $\lambda_1 = 1.5$.


Fig. 7: Variation of pressure rise Δp with Q for fixed $\varepsilon = 0.01$, $M = 0.5$, $t = 0.1$, $\theta = 50^0$, $\phi = 0.2$, $V = 0.5$, $\lambda_1 = 1.5$.

Fig. 7 indicates the effect of the parameters λ_1 and δ upon pressure rise. This plot reveals that the peristaltic pumping area lies in between $Q \in [0, 0.6]$, the retrograde pumping appears in the part $Q \in [-1, 0]$ and the augmented pumping region is $Q \in [0.6, 2]$. The pressure gradient dp/dz for the parameters M and δ is drawn in Fig. 8.

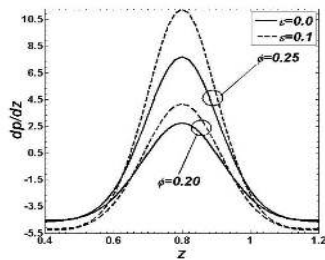It is measured from this figure that pressure gradient is in linear relation with both of the parameters in
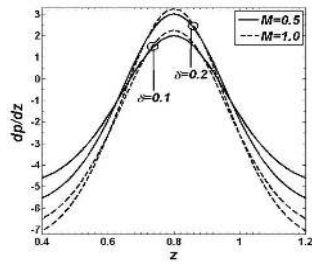
Fig. 8: Variation of pressure gradient dp/dz with z for fixed $\varepsilon = 0.01$, $V = 0.3$, $t = 0.3$, $\theta = 50^0$, $\phi = 0.1$, $Q = 0.5$, $\lambda_1 = 1.5$.
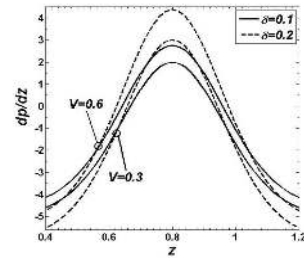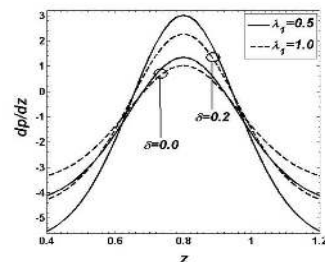

Fig. 11: Variation of pressure gradient dp/dz with z for fixed $\varepsilon = 0.01$, $Q = 0.5$, $t = 0.3$, $\theta = 50^0$, $M = 0.5$, $\phi = 0.1$, $\lambda_1 = 0.5$.

narrowest parts of the cylinders but inverse relation is seen in the wider parts. The variation of pressure gradient with the parameters ϕ and ε is very much similar to that of the parameters M and δ and is shown in Fig. 9.

It can be observed from Figs. 10 and 11 that the pressure gradient increases with the parameters Q and V, while when δ is increased the pressure gradient decreases on the left and right sides but increases at the centre of the cylinders. It is also seen that the variation of pressure gradient remains same in the two sides of the channel and become different at the central part with changing V but this variation remains same throughout for the parameter Q. The pressure gradient graph for the parameters λ_1 and δ is drawn in the Fig. 12.

Fig. 9: Variation of pressure gradient dp/dz with z for fixed $\delta = 0.1$, $V = 0.3$, $t = 0.3$, $\theta = 50^0$, $M = 0.5$, $Q = 1$, $\lambda_1 = 1.5$.

The only difference is that the pressure gradient is minimum on the left and right sides of the cylinder while appears maximum at the centre. It means that flow can easily pass without imposition of large pressure gradient in the two sides of the channel while much pressure gradient is required to maintain the flux in the central part near $z = 0.8$. This is in good agreement with the physical condition.
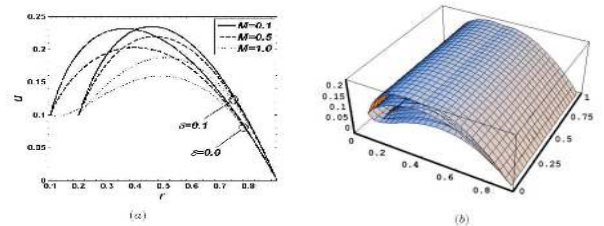

Fig. 12: Variation of pressure gradient dp/dz with z for fixed $\varepsilon = 0.01$, $Q = 0.5$, $t = 0.3$, $\theta = 50^0$, $M = 0.5$, $\phi = 0.1$, $V = 0.3$.

It is seen here that the pressure gradient increases with δ at the middle but decreases at the two sides of the cylinders. However, the effect of the parameter λ_1 is totally opposite with that of δ.
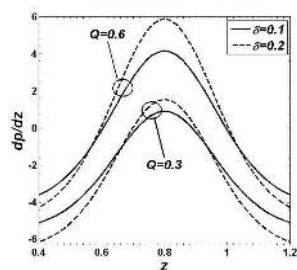

Fig. 10: Variation of pressure gradient dp/dz with z for fixed $\varepsilon = 0.01$, $V = 0.3$, $t = 0.3$, $\theta = 50^0$, $M = 0.5$, $\phi = 0.1$, $\lambda_1 = 0.5$.
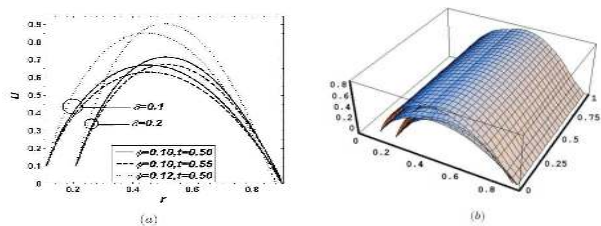

Fig. 13: Variation of velocity profile u with r for fixed $\varepsilon = 0.1$, $Q = 0.5$, $t = 0.5$, $z = 0$, $V = 0.1$, $\theta = 50^0$, $\phi = 0.1$, $\lambda_1 = 1.5$.

The Fig. 13 shows that the velocity field is an increasing function of the parameter δ while decreasing with the parameter M. The velocity field is in inverse relation with Q but have a direct variation with ε (See Fig. 14).
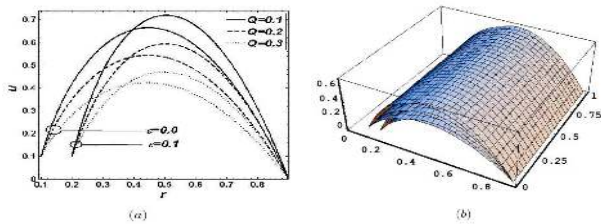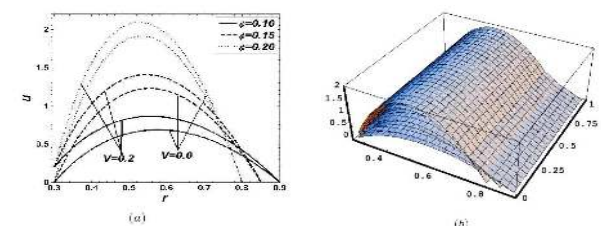

Fig. 14: Variation of velocity profile u with r for fixed $\delta = 0.1$, $M = 0.5, t = 0.5, z = 0, V = 0.1, \theta = 50^0, \phi = 0.1, \lambda_1 = 1.5$.

Fig. 15: Variation of velocity profile u with r for fixed $Q = 0.1$, $M = 0.5, \varepsilon = 0.01, z = 0, V = 0.1, \theta = 50^0, \lambda_1 = 1.5$.

It is observed from Fig. 15 that the velocity distribution is increasing with δ and ϕ while reducing for t.


Fig. 16: Variation of velocity profile u with r for fixed $Q = 0.1$, $M = 0.5, t = 0.5, \varepsilon = 0.1, z = 0, \delta = 0.2, \theta = 50^0, \lambda_1 = 1.5$.

Fig. 16 shows that the velocity profile is linearly changing with ϕ and V.

From Fig. 17, it is measured that velocity is lessened with the increasing effect of the parameter λ_1. It is also observed that velocity is decreasing function of δ in the region $r \in [0.2, 0.4]$, while increasing on the rest of the domain.
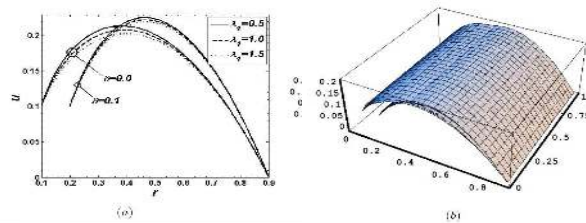

Fig. 17: Variation of velocity profile u with r for fixed $Q = 0.5$, $M = 0.5, t = 0.5, \varepsilon = 0.1, z = 0, \theta = 50^0, \phi = 0.1, V = 0.1$.
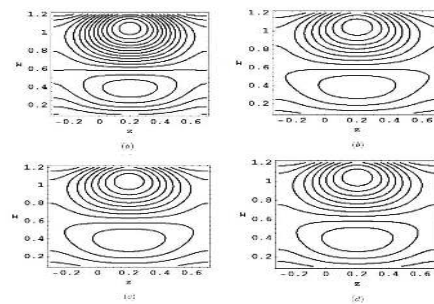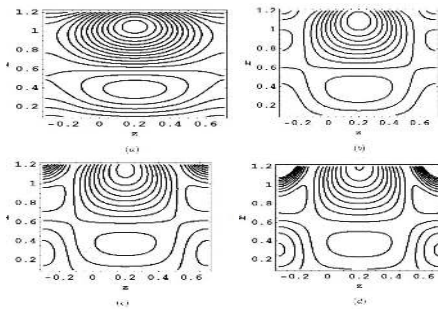

Fig. 18: Stream lines for different values of M. (a) for $M = 0.3$, (b) for $M = 0.4$, (c) for $M = 0.5$, (d) for $M = 0.6$. The other parameters are $\varepsilon = 0.4, V = 0.3, t = 0.2, \theta = 50^0, \phi = 0.05$, $Q = 0.6, \delta = 0.05, \lambda_1 = 1$.

Fig. 18 is drawn to see the stream lines for the parameter M. It is measured from this figure that numbers of bolus are not changing but size is increasing with the increasing effects of M in the bottom of the cylinder, while bolus are lessened in number when seen in the upper part. The boluses are reduced both in size and number when seen for the parameter Q in both parts of the geometry (see Fig. 19).
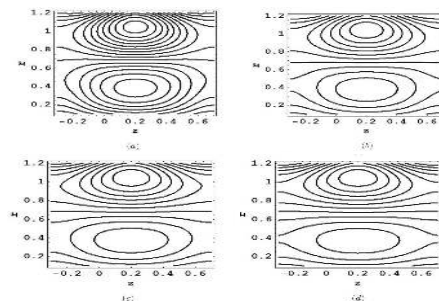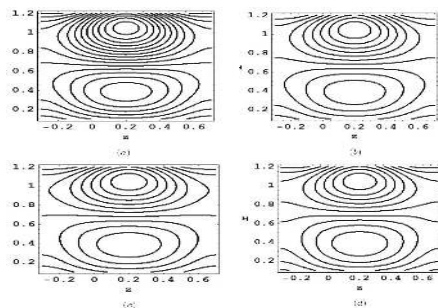

Fig. 19: Stream lines for different values of Q. (a) for $Q = 0.6$, (b) for $Q = 0.7$, (c) for $Q = 0.8$, (d) for $Q = 0.9$. The other parameters are $\varepsilon = 0.4, V = 0.3, t = 0.2, \theta = 50^0, \phi = 0.05$, $M = 1, \delta = 0.05, \lambda_1 = 1$.

Fig. 20: Stream lines for different values of ϕ. (a) for $\phi = 0.05$, (b) for $\phi = 0.1$, (c) for $\phi = 0.15$, (d) for $\phi = 0.2$. The other parameters are $\varepsilon = 0.4$, $V = 0.3$, $t = 0.2$, $\theta = 50^0$, $Q = 0.6$, $M = 0.4$, $\delta = 0.05$, $\lambda_1 = 1$.

It is seen from Fig. 20 that the numbers of bolus are decreasing with different values of the parameter ϕ in both sides of the cylinder but in the lower half of the channel, the bolus becomes smaller with increasing magnitude of the parameter ϕ. Fig. 21 reveals the fact that when we increase the value of the parameter λ_1, the boluses decreased in number but expanded in size.

Fig. 21: Stream lines for different values of λ_1. (a) for $\lambda_1 = 0.5$, (b) for $\lambda_1 = 0.7$, (c) for $\lambda_1 = 0.9$, (d) for $\lambda_1 = 1.1$. The other parameters are $\varepsilon = 0.4$, $V = 0.3$, $t = 0.2$, $\theta = 50^0$, $Q = 0.6$, $M = 1$, $\delta = 0.05$, $\phi = 0.05$.

Acknowledgment

References

[1] S. Srinivas and R. Gayathri, Peristaltic transport of a Newtonian fluid in a vertical asymmetric channel with heat transfer and porous medium, Appl. Math. Comput., **215**, 185 (2009).

[2] M. Kothandapani and S. Srinivas, Peristaltic transport of a Jeffrey fluid under the effect of magnetic field in an asymmetric channel, Int. J. Nonlinear. Mech., **43**, 915 (2008).

[3] Sankar, D.S., Hemalatha, K.: Pulsatile flow of Herschel–Bulkley fluid through catheterized arteries – A mathematical model. Appl. Math. Model. **31**, 1497–1517 (2007)

[4] O. Eytan and D. Elad, Analysis of intra-uterine fluid motion induced by uterine contractions, Bull. Math. Biol., **61**, 221 (1999).

[5] Kh.S. Mekheimer, Y. Abdelmaboud, Peristaltic flow of a couple stress fluid in an annulus: Application of an endoscope, Physics A.,2403, 387 (2008).

[6] S. K. Pandey and M. K. Chaube, Peristaltic flow of a micropolar fluid through a porous medium in the presence of an external magnetic field, Commun Nonlinear Sci. Numer. Simul., **16**, 3591 (2011).

[7] Kh. S. Mekheimer, Peristaltic flow of blood under effect of a magnetic field in a non-uniform channels, Appl. Math. Comput., **153**, 763 (2004).

[8] S. Nadeem and N. S. Akbar, Influence of radially varying MHD on the peristaltic flow in an annulus with heat and mass transfer, Taiwan Institute of Chem. Eng., **41**, 286 (2010).

[9] S. Nadeem and N. S. Akbar, Effects of heat and chemical reactions on peristaltic flow of Newtonian fluid in a diverging tube with inclined MHD, Asia Pascific J. of Chem. Eng., **6**, 659 (2011).

[10] R. Ellahi, A. Riaz, S. Nadeem and M. Ali, Peristalic flow of Carreau fluid in a rectangular duct through a porous medium, Mathematical Prob. in Eng., **2012**, 24, Article ID 329639, (2012).

[11] A. Afsar Khan, R. Ellahi and K. Vafai, Peristaltic transport of Jeffrey fluid with variable viscosity through a porous medium in an asymmetric channel, Advances in Mathematical Phys., **2012**, 15, Article ID 169642, (2012).

[12] Kh. S. Mekheimer and A. N. Abdel-Wahab, Net annulus flow of a compressible viscous liquid with peristalsis, J. Aerospace Eng., **25** , 660 (2012).

[13] J. M. Nouri, H. Umur and J. H. Whitelaw, Flow of Newtonian and non-Newtonian fluids in concentric and eccentric annuli, J. Fluid Mech., **253**, 617 (1993).

[14] I. C. Walton and S. H. Bittlestone, The axial flow of a Bingham plastic in a narrow eccentric annulus, J. Fluid Mech., **222**, 39 (1991).

[15] Kh. S. Mekheimer, Y. Abdelmaboud and A. I. Abdellateef, Peristaltic transport through an eccentric cylinders: Mathematical model, Appl. Bionics Biomech., 10.3233/ABB-2012-0071

[16] J. H. He, Homotopy perturbation method for solving boundary value problems, Phys. Lett. A., **350**, 87 (2006).

[17] A. Saadatmandi, M. Dehghan and A. Eftekhari, Application of He's homotopy perturbation method for non-linear system of second-order boundary value problems, Nonlinear Anal. Real World App., **10**, 1912 (2009).

Appl. Math. Inf. Sci. **7**, No. 4, 1441-1449 (2013) / www.naturalspublishing.com/Journals.asp

1449

Dr. R. Ellahi is a Fulbright Fellow in the University Of California Riverside, USA and also founder Chairperson of the Department of Mathematics and Statistics at IIUI, Pakistan. He has several awards and honors on his credit: Fulbright Fellow, Productive Scientist of Pakistan, Best University Teacher Award by higher education commission (HEC) Pakistan, Best Book Award, and Valued Reviewer Award by Elsevier. He is also an author of six books and editor of two international journals.

Mr. Arshad Riaz is working as a PhD Scholar in the department of Mathematics at International Islamic University, Islamabad under the supervision of Dr. Rahmat Ellahi. He obtained his MS degrees with distinction and published his research articles in internationally refereed journals.

Dr. Sohail Nadeem is an Associate Professor at Quaid-i-Azam University Islamabad. He is recipient of Razi-ud-Din gold medal by Pakistan Academy of Sciences and Tamgha-i-Imtiaz by the President of Pakistan. He is young fellow of TWAS, Italy.

Dr. M. Mushtaq is an Assistant Professor in the Department of Mathematics, University of Engineering & Technology, Lahore Pakistan. His field of research is Computational Fluid Dynamics. His research articles have been published in national and international journals.